Bond-order potential for molybdenum: Application to dislocation behavior

M. Mrovec,[1,*] D. Nguyen-Manh,[2,†] D. G. Pettifor,[2] and V. Vitek[1,‡]
[1]*Department of Materials Science and Engineering, University of Pennsylvania, Philadelphia, Pennsylvania 19104-6267, USA*
[2]*Department of Materials, University of Oxford, Parks Road, Oxford OX1 3PH, United Kingdom*
(Received 19 October 2003; revised manuscript received 20 January 2004; published 24 March 2004)

The bond-order potential (BOP) for transition metals is a real-space semiempirical description of interactions between the atoms, which is based on the tight-binding approximation and the *d*-band model. This scheme provides a direct bridge between the electronic level modeling and the atomistic modeling, where the electronic degrees of freedom have been coarse grained into many-body interatomic potentials. In this paper we construct BOP in which both the attractive and the repulsive contributions to the binding energy are environmentally dependent due to both the nonorthogonality of the orbitals and the breathing of the screening charges. The construction of the BOP is described and tested in detail. First, the energies of alternative crystal structures (A15, fcc, hcp, simple cubic) are calculated and compared with those evaluated *ab initio*. The transferability of the BOP to atomic configurations that deviate significantly from the bcc lattice is studied by computing the energies along tetragonal, trigonal, and hexagonal transformation paths. Next, the phonon spectra are evaluated for several symmetrical crystallographic directions and compared with available experiments. All these calculations highlight the importance of directional bonding and the investigation of phonons demonstrates that the environmental dependence of the bond integrals is crucial for the phonons of the *N* branch not to be unphysically soft. Finally, the constructed BOP was applied in the modeling of the core structure and glide of the $1/2\langle 111\rangle$ screw dislocation. The calculated structure of the core agrees excellently with that found in the recent *ab initio* calculations and the observed glide behavior not only agrees with available *ab initio* data but is in agreement with many experimental observations and explains the primary reason for the breakdown of the Schmid law in bcc metals.

DOI: 10.1103/PhysRevB.69.094115 PACS number(s): 61.72.Bb, 71.15.Nc, 71.20.Be, 62.25.+g

I. INTRODUCTION

Many physical properties of crystalline materials, in particular their mechanical behavior, are controlled by crystal defects, such as point defects, dislocations, grain boundaries, and other interfaces. Frequently, the atomic structure of these defects plays a critical role. For example, it is now accepted that dislocation core phenomena in materials with structures more complex than close-packed fcc often bring about unexpected deformation modes, strong and unusual dependencies of the flow stress on temperature, strain rate, and orientation of the crystal with respect to the loading axes (for reviews see, e.g., Refs. 1–3). The bcc transition metals, including iron at ambient and low temperatures, and their alloys were the first materials in which such effects have been recognized and systematically studied (for reviews see Refs. 4–8). Theoretical treatment of such complex phenomena and related structures of extended defects is very demanding and it is the atomic-level computer modeling that is the most promising approach in such research.

The principal precursor of all atomic-level studies, in particular those involving systems composed of a large number of atoms that do not form an ideal lattice, is a reliable description of atomic interactions. The state-of-the-art first-principles methods based on the density-functional theory (DFT), which require only a few fundamental physical constants as input, provide such a description most reliably. However, these rigorous calculations are limited either to ideal structures without any defects or to studies of periodic arrays of very closely spaced defects, owing to the application of periodic boundary conditions and feasible block sizes that contain couple of hundred of atoms. Studies of large and complex systems require approximations and simplifications when describing atomic interactions that may, however, obliterate some important features of bonding. For this reason, the most challenging aspect of materials modeling is the choice of the description of atomic interactions that correctly and with sufficient accuracy reflects the physics of bonding in any specific case, while at the same time it is computationally treatable for large systems of particles.

In the last decade the most commonly used have been central-force many-body potentials,[9] in particular the embedded-atom method[10,11] and Finnis-Sinclair potentials.[12,13] These schemes are very good approximations for simple and noble metals in which the bonding is almost nearly free-electron-like (NFE).

However, in transition metals and intermetallic compounds based on transition metals, which are materials that are important in both structural and functional applications,[14–18] the bonding has a mixed NFE and covalent character. Indeed, it has been established a long time ago that it is the filling of the *d* band that controls the cohesion and hence the particular ground-state structure which a transition metal takes.[19,20] This bonding which is mediated by the *d* electrons is covalent in character. In particular, such covalent bonding is shown to be strongest for bcc transition metals in groups V and VI of the periodic table, i.e., in the transition metals with the *d* band about half filled. This aspect of bonding is even more important in transition-metal based intermetallic alloys, such as TiAl or $MoSi_2$, where strong directional *p*-*d* bonds are formed between the *sd*-valent transition metals and *sp*-valent elements.[21–24]

Nonetheless, central-force potentials of the Finnis-Sinclair type have been constructed for elemental bcc transition metals[25] and used, for example, in studies of dislocation cores.[26,27] These calculations, together with earlier studies that employed pair potentials (for reviews see Refs. 28 and 7), detected a number of general features of dislocation cores and their response to applied stresses that can be expected in all materials with the bcc lattice. However, such simple models of atomic interactions fail to identify subtle differences in properties of specific materials. This has been demonstrated most tenaciously by recent *ab initio* calculations of the structure of the core of screw dislocations in molybdenum[29] that revealed a different type of the dislocation core than calculations employing Finnis-Sinclair-type potentials.[26,27] As will be discussed in more detail in Sec. V of this paper, this discord is most likely a consequence of the neglect of the directional character of covalent bonding in the latter case.

Various approximate schemes that include noncentral forces have been advanced in recent years. They range from empirical modified embedded-atom method[30] to the approach based on perturbation expansions employed in the framework of first-principles generalized pseudopotential theory.[31,32] In this paper, we focus on the many-atom bond-order potentials (BOP's) that give an exact representation of the bond energy within the chemically intuitive tight-binding (TB) approximation to the quantum-mechanical electronic structure[33–35] and retain thus the angular character of bonding. This method, using an orthogonal TB basis and two-center bond integrals has been implemented in the Oxford order-N (OXON) package.[36] The BOP's provide a direct bridge between the electronic level modeling, with its full treatment of the electronic degrees of freedom, and the atomistic modeling, where the electronic degrees of freedom have been coarse grained into many-body interatomic potentials. Apart from the quantum-mechanical character, another significant advantage of BOP's is that modeling of extended defects, which requires a large number of atoms, can be performed in real space. This broadens the range of solvable problems and avoids using periodic boundary conditions necessary in k space methods. Within this BOP scheme, the Hellmann-Feynman theorem can be used to evaluate forces on the atoms and the computational effort scales linearly with the number of atoms in the system, decreasing thus dramatically the computational time. These potentials have now been developed for Ti (Refs. 37 and 38) and Ti-Al alloys.[39] Their application led to an explanation of the preference for prism slip in titanium and gives a prediction of energies of stacking-fault-like defects and dislocation core structures that agree with experimental measurements and *ab initio* calculations in TiAl.

Despite the above-mentioned successes, the BOP's still suffer from general uncertainty, common to all parametrized TB schemes: How to choose in the most confident and reliable way the semiempirical bond integrals[40] that enter the method. In particular, it is of primary importance that the dependence of these integrals on separation of atoms and bond angles is transferable to varying environments. It has been recognized recently that for the orthogonal TB model to be robust and transferable to different situations, the two-center bond integrals have to be environment dependent.[41–46] While a purely empirical treatment of this dependence is possible, it may lead to introduction of such a large number of fitting parameters that the application of an environmentally dependent TB method becomes an overwhelming task, in particular for multicomponent systems.

In this paper we avoid this problem by using analytic expression for the environmental dependence of the tight-binding bond integrals that we derived recently.[47] These expressions were obtained by starting from a nonorthogonal tight-binding representation and using BOP methodology to invert the overlap matrix.[48,49] The resultant two-center bond integrals are explicitly dependent on the local environment not only through the bond lengths or distance but also through the bond angles via a so-called screening function. We will see that these analytic expressions may be fitted to reproduce accurately the values of the screened bond integrals that are obtained numerically from the tight-binding linearized-muffin-tin-orbitals (TB-LMTO) theory.[50] We will demonstrate that the inclusion of this screening function is critical for modeling bcc Mo because in this case second-nearest neighbors play an important role unlike the case of close-packed Ti and TiAl which had been considered previously.[37–39]

This paper is organized as follows. In Sec. II, we review the theoretical background of BOP's and discuss specific implementation of the analytic screened bond integrals into the BOP scheme. Then in Sec. III we apply this approach in the construction of screened bond-order potentials for bcc Mo. Testing of these potentials that comprises calculations of structural energy differences, deformation paths transforming the bcc lattice to other structures, vacancy formation energies, and calculation of phonon spectra is presented in Sec. IV. Results of these calculations are compared with available DFT-based calculations and/or experiments. In order to assess the importance of the screening, we also provide a comparison with predictions of a bond-order potential without the screening of the bond integrals (labeled as BOP_0). In Sec. V we apply the constructed BOP in the study of the core structure and glide of screw dislocations in Mo. This involves investigation of the effect of applied shear stresses and analysis of the results in terms of γ surfaces[3] and includes comparison with recent *ab initio* calculations.[29,51] Preliminary results have been published in Refs. 52 and 53. Finally, Sec. VI summarizes the most important aspects of the BOP for bcc Mo and discusses their applicability in large-scale atomistic studies.

II. BOND-ORDER POTENTIAL FORMALISM

Following recent detailed description of the bond-order potential formalism,[37–39,54] based on the TB bond model,[20,34,55] the binding energy of transition metals and their alloys can be written as

$$U = U_{bond} + U_{env} + U_{pair}. \tag{1}$$

U_{bond} is the attractive bond energy, U_{env} is the repulsive environmentally dependent contribution that originates from the strong core repulsion which the valence sp electrons ex-

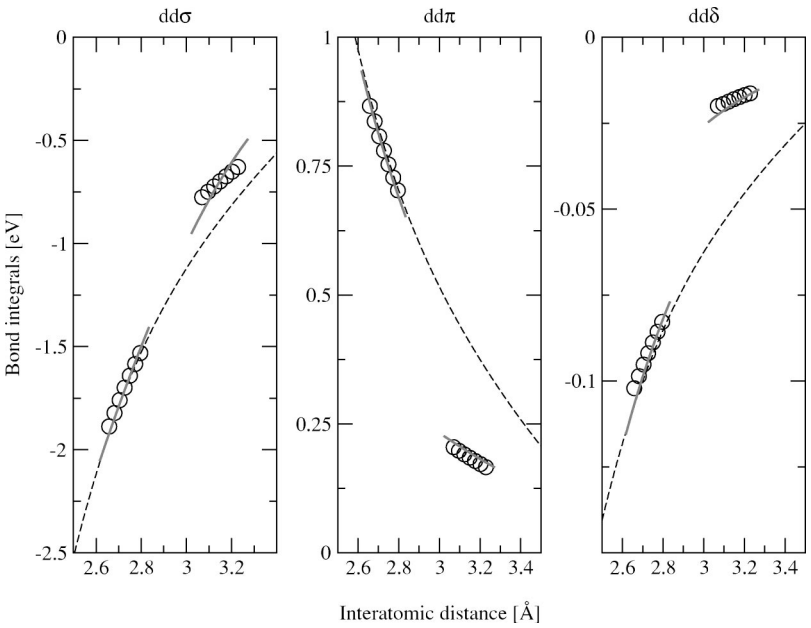

FIG. 1. Radial dependencies of $dd\sigma$, $dd\pi$, and $dd\delta$ bond integrals. Circles: Values calculated using TB-LMTO for the first- and second-nearest neighbors in bcc Mo with varying lattice parameter. Dashed curves: unscreened bond integrals. Full curves: screened bond integrals.

perience in transition metals and their alloys,[56,57] and U_{pair} is the usual pairwise contribution arising from the overlap repulsion and electrostatic interaction between the atoms.[58] Within the two-center, orthogonal TB model the bond energy can be considered as a sum of contributions from individual $i-j$ bonds, U_{bond}^{ij}, so that

$$U_{bond}=\frac{1}{2}\sum_{i,j\neq i} U_{bond}^{ij}, \tag{2}$$

where

$$U_{bond}^{ij}=\sum_{\alpha\beta} 2H_{i\alpha,j\beta}\Theta_{j\beta,i\alpha}. \tag{3}$$

The prefactor 2 accounts for spin degeneracy and $H_{i\alpha,j\beta}$ and $\Theta_{j\beta,i\alpha}$ are the Hamiltonian and bond-order matrix elements, respectively, which are associated with individual bonds $i-j$ and corresponding atomic orbitals α and β. The Hamiltonian matrix elements $H_{i\alpha,j\beta}$ are defined in terms of the usual two-center Slater-Koster bond integrals.[40] The bond-order matrix element $\Theta_{i\alpha,j\beta}$ is defined as one-half of the difference between the number of electrons in the bonding state $|+\rangle=(1/\sqrt{2})(|i\alpha\rangle+|j\beta\rangle)$ compared to the antibonding state $|-\rangle=(1/\sqrt{2})(|i\alpha\rangle-|j\beta\rangle)$.

The bond integrals $dd\sigma$, $dd\pi$, and $dd\delta$ that enter the TB Hamiltonian are fitted to the values which are obtained from first-principles TB-LMTO.[47,50,59] These are plotted for the first- and second-nearest neighbors in bcc Mo as the open circles in Fig. 1. The seven points in each neighboring shell correspond to a range of seven different values about the experimental equilibrium volume V_0, namely V_0, $(1\pm0.025)V_0$, $(1\pm0.05)V_0$, and $(1\pm0.075)V_0$. We see that there is a marked discontinuity between the distance dependencies of the first and second shells for the $dd\pi$ and $dd\delta$ bond integrals, in particular. This phenomenon is the result of the screening of the bond integrals by the local environment. It was first captured by the empirical environment-dependent tight-binding scheme.[45]

In this paper we represent this environment dependence of the screened d-bond integrals $\tilde{\beta}_\tau^{ij}$ through the analytic expression derived from nonorthogonal TB,[47] namely

$$\tilde{\beta}_\tau^{ij}=\beta_\tau(R_{ij})(1-S_\tau^{ij}), \tag{4}$$

where $\tau=\sigma$, π, or δ. The unscreened d-bond integrals $\beta_\tau(R_{ij})$ are pairwise functions that are assumed to take a generalized Goodwin-Skinner-Pettifor (GSP) form,[60] namely

$$\beta_\tau(R)=\beta_\tau(R_0)\left(\frac{R_0}{R}\right)^{n_a}\times\exp\left\{n_b\left[\left(\frac{R_0}{R_c}\right)^{n_c}-\left(\frac{R}{R_c}\right)^{n_c}\right]\right\}, \tag{5}$$

where R_0 is the equilibrium first-nearest-neighbor distance; n_a, n_b, n_c, and R_c are fitting parameters. The screening functions S_τ^{ij}, which result from the screening of the $i-j$ d bond by the s-valence orbitals on the neighboring atoms k, take the form

$$S_\tau^{ij}=\frac{(c_1^{ij})_\tau-(\overline{\mu_2})_\tau}{1+O_\tau^2(R_{ij})-2(\overline{\mu_2})_\tau}, \tag{6}$$

where $O_\tau(R_{ij})$ is the d-d overlap integral between orbitals centered on atoms i and j. c_1 is the interference contribution that results from the electrons hopping between the σ, π, or δ valence d orbitals on atom i and j via the surrounding lattice, as illustrated schematically in Fig. 2. The dominant contribution is the two-hopping path from $i\rightarrow k\rightarrow j$ via an unscreened bond integral $\beta_{ds\sigma}$ and overlap integral $O_{sd\sigma}$. A much smaller contribution results from three hops from $i\rightarrow k\rightarrow i\rightarrow j$. Higher terms are negligible. The diagrams in Fig. 2 can be summed up to give

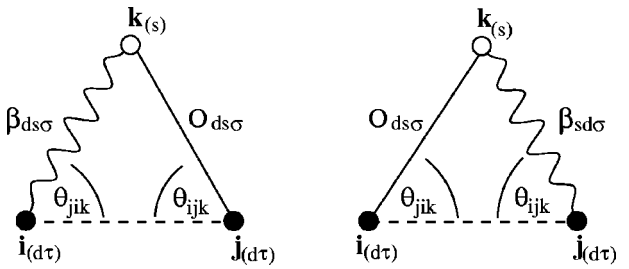

FIG. 2. Schematic depiction of the dominant interactions in the interference $(c_1^{ij})_\tau$ arising from hopping via the bond integral (wavy line) and overlap integral (straight line).

$$(c_1^{ij})_\tau = A_\tau \sum_{k\neq i,j} [(1+\delta_{\tau 0})/4] \frac{1}{\beta_\tau(R_{ij})} \{[\beta_{ds\sigma}(R_{ik}) O_{sd\sigma}(R_{kj}) + O_{ds\sigma}(R_{ik})\beta_{sd\sigma}(R_{kj})] g_\tau(\theta_{jik}) g_\tau(-\theta_{ijk}) - [\beta_{ds\sigma}(R_{ik}) O_{sd\sigma}(R_{ki}) O_\tau(R_{ij}) g_\tau^2(\theta_{jik}) + O_\tau(R_{ij}) O_{ds\sigma}(R_{jk}) \beta_{sd\sigma}(R_{kj}) g_\tau^2(\theta_{ijk})]\}, \quad (7)$$

where $\delta_{\tau 0}$ equals 1 for $\tau=\sigma$ but 0 for $\tau=\pi$ or δ. A_τ equals 1 in our original paper[47] and in this study (see Sec. III) it is used as a fitting parameter. The sd-bond integral $\beta_{ds\sigma}$ takes the GSP form of Eq. (5). We have assumed that the overlap integrals fall off with distance in the same way as the corresponding bond integrals, so that each overlap integral introduces a single new fitting parameter $O(R_0)/\beta(R_0)$. As might be expected the interference contributions are dependent on the angular character of the d bond that is being screened through the angular functions

$$g_\sigma(\theta) = (1/4)(1+3\cos 2\theta),$$

$$g_\pi(\theta) = (\sqrt{3}/2)\sin 2\theta,$$

$$g_\delta(\theta) = (\sqrt{3}/4)(1-\cos 2\theta). \quad (8)$$

The screening function S_τ^{ij} in Eq. (6) is further weakly renormalized through the presence of the two-hop second-moment contribution $(\overline{\mu_2})_\tau = \frac{1}{2}[(\mu_2^i)_\tau + (\mu_2^j)_\tau]$, where

$$(\mu_2^i)_\tau = O_\tau^2(R_{ij}) + A_\tau \sum_{k\neq i,j} [(1+\delta_{\tau 0})/2] O_{ds\sigma}^2(R_{ik}) g_\tau^2(\theta_{jik}). \quad (9)$$

The bond order and the bond energies in Eq. (3) are obtained from the OXON package.[36] This real-space method requires the introduction of a fictitious temperature in order to dampen down the long-range Friedel oscillations in metals, thereby guaranteeing the validity of the Hellmann-Feynman theorem when evaluating forces;[36] for more details see also Ref. 37. We have found that sufficient accuracy is provided by $k_BT=0.3$ eV if BOP theory retains contributions up to the ninth moment in the local electronic density of states. The individual forces on all the atoms in our calculations are converged to better than 0.01 eV/Å. The bond-order matrix is evaluated under the assumption of local charge neutrality which is an excellent approximation for metallic systems. This is achieved by adjusting self-consistently the on-site atomic energy levels on all the Mo sites.

The environmentally dependent term U_{env} represents the repulsion due to the valence s and p electrons being squeezed into the ion core regions under the influence of the large covalent d-bonding forces. It can be described by a screened Yukawa-type potential:[57]

$$U_{env} = \frac{1}{2} \sum_{i,j\neq i} \frac{B}{R_{ij}} \exp[-\lambda_{ij}(R_{ij} - 2R_{core})], \quad (10)$$

where R_{core} is the core radius and $\lambda_{ij}=(1/2)(\lambda_i+\lambda_j)$. The screening exponent λ_{ij} is dependent on the local density and environment of atoms i and j. Here we model the environmental dependence through an embedded-atom-type expression by writing

$$\lambda_i = \lambda_0 + \left[\sum_{k\neq i} C \exp(-\nu R_{ik})\right]^{1/m}, \quad (11)$$

where λ_0 (the unscreened value of the exponent), C, ν, and m are all adjustable parameters. These parameters are different for different chemical species and determined by fitting the experimental values of the Cauchy pressures.[39,57]

The final contribution to the binding energy, U_{pair}, arises nominally from the overlap repulsion and the electrostatic interaction between the atoms. It can be expressed as

$$U_{pair} = \frac{1}{2} \sum_{i\neq j} V(R_{ij}), \quad (12)$$

where $V(R_{ij})$ is a pair potential. For this pair potential we employ here the same functional form as that used in Ref. 13 when constructing Finnis-Sinclair potentials, namely a sum of cubic splines:

$$V(R_{ij}) = \sum_k A_k (R_k - R_{ij})^3 H(R_k - R_{ij}) \quad (13)$$

with $H(x)$ the Heaviside step function. The node points R_k and A_k are used as fitting parameters. The functional form of the pair potential assures that $V(R_{ij})$, as well as its first and second derivatives, are everywhere continuous and equal to zero at the cutoff distance R_1. The parameters in this potential are obtained by fitting those elastic constants that remain after fixing the Cauchy pressures, the cohesive energy, and equilibrium lattice parameters.

III. FITTING BOND-ORDER POTENTIAL FOR MOLYBDENUM

The fitting of parameters entering the BOP was done in the same way as in Ref. 39. An important aspect of this fitting scheme is that the three parts of the energy in Eq. (1) are developed independently and sequentially. First, U_{bond} is constructed based solely on *ab initio* data with no empirical input. Next U_{env} is contrived to reproduce the Cauchy pressure $C_{12}-C_{44}$ and finally, the pair potential is fitted to repro-

TABLE I. Parameters for the screened bond integrals.

	R_c (Å)	$\beta_\tau(R_0)$(eV)	$O_\tau(R_0)$	n_a	n_b	n_c
$dd\sigma$	1.873	−1.6200	0.0442	0.179	0.179	4.426
$dd\pi$	0.590	0.8900	−0.0352	0.0	1.0	1.0
$dd\delta$	0.500	−0.1360	0.0253	0.0	1.0	1.0
$sd\sigma$	0.850	−1.1547	0.1600	0.0	1.0	1.0

duce the lattice parameter, remaining elastic moduli and cohesive energy.

U_{bond} is the essential and most complex part of the BOP in which the underlying electronic structure comes into play. Since *d*-*d* bonding governs the cohesion of bcc transition metals, only *d* electrons have been included explicitly into U_{bond}. The validity of this approximation has been tested by several authors[20,36] and the principal justification is that the electronic densities of states in bcc transition metals calculated in this approximation show the same dominant features as those determined by *ab initio* all-electron codes, in particular the characteristic bimodal shape and pseudogap. Within this orthogonal TB *d*-band model the bond part involves only the $dd\sigma$, $dd\pi$, and $dd\delta$ two-center bond integrals with the angular dependence of the intersite Hamiltonian matrix elements taking the Slater and Koster[40] form. The distance dependence of the bond integrals needs to be represented by a continuous differentiable functional form and for this purpose we have employed the generalized GSP function given by Eq. (5).

The first-principles TB-LMTO method, which utilizes a small basis of atom-centered, short-ranged orbitals, enables us to establish a direct link with the semiempirical, parametrized tight-binding methods.[61] In order to determine the dependence of the screened bond integrals, $\tilde{\beta}_\tau$, on the separation of atoms we evaluated them numerically for different volumes of the unit cell using this *ab initio* method (see circles in Fig. 1). We see that the bond integrals display a marked discontinuity between first- and second-nearest neighbors and, as explained in Sec. II, this can be captured by including their screening arising from the nonorthogonality of the orbitals. This requires the introduction of a small number of parameters that enter the screening function defined by Eqs. (6)–(9). Specifically, these are the bond integral $\beta_{sd\sigma}$ (since the screening is assumed to be due to the *s*-valence electrons on the atoms neighboring to the bond) and the overlap integral $O_{sd\sigma}$ together with the *dd* overlap integrals $O_{dd\tau}$, where τ corresponds to σ, π, and δ, respectively. The overlap integrals have the same scaling dependencies as the corresponding unscreened bond integrals so that they are also represented by the generalized GSP function defined by Eq. (5) with the same parameters n_a, n_b, n_c, and R_c as for the nonscreened bond integrals β_τ. An additional fitting parameter A_τ appears in both the interference and second-moment contributions to the screening in Eqs. (7) and (9).

The solid curves in Fig. 1 show the accuracy of the fit achieved by our analytic expression for the screened bond integrals. This fit was attained by setting the parameters as given in Table I together with $A_\sigma = A_\pi = 1$ and $A_\delta = 0.32$. The nearest-neighbor equilibrium spacing was taken as $R_0 = 2.7256$ Å.

Magnitudes of bond and overlap integrals decrease rapidly with increasing interatomic distance and in bcc structures only first- and second-nearest neighbor contributions are significant. Hence, both the bond and overlap integrals have been cut off between the second and third neighbors. The fact that these integrals are short ranged also assures that the model is not too intensive computationally. In order to guarantee that the bond and overlap integrals decrease smoothly to zero, the GSP function is employed for $R < R_1$ and is augmented with a polynomial of fifth order for $R_1 < R < R_{cut}$,

$$P(R) = C_0 + (R-R_1)[C_1 + (R-R_1)[C_2 + (R-R_1)[C_3 + (R-R_1)[C_4 + (R-R_1)[C_5 + (R-R_1)]]]]]. \quad (14)$$

The distance R_1, at which this tail is attached to the GSP function, is chosen such that no unphysical ''humps'' occur on the R dependence of the bond integrals. The coefficients of the polynomial spline in Eq. (14) are computed automatically in the OXON code so that the function and its first and second derivatives are continuous at $R = R_1$ and zero at $R = R_{cut}$. The best choice of R_1 and R_{cut} was found to be the same for all the bond and overlap integrals, specifically 3.3 Å and 4.3 Å, respectively.

Resulting analytical representations of the radial parts of bond integrals when screening is not included (β_τ) are shown in Fig. 1 as dashed curves. It is seen from this figure that while this representation could be acceptable for $dd\sigma$ integrals, it is not for $dd\pi$ and $dd\delta$ integrals that display a marked discontinuity between first- and second-nearest neighbors. In contrast, the analytic screening function reproduces very closely the bond integrals determined by the TB-LMTO. This is demonstrated in Fig. 1 by solid curves that represent the screened bond integrals ($\tilde{\beta}_\tau$). Obviously, since the environment of the first- and second-nearest neighbors is not the same, the values of the screening function for the first and second neighbors are also different. Consequently, the screened bond integrals are not continuous and display a large discontinuity between the first- and second-nearest neighbors in the case of $dd\pi$ and $dd\delta$ whereas the discontinuity of $dd\sigma$ is only small. This behavior can be traced directly to the angular dependence of the screening function. The bcc lattice has nearest-neighbor bond angles $\Theta = \cos^{-1}(1/\sqrt{3})$ so that the angular term $g_{2\sigma} = (1/4)(1 + 3\cos 2\theta)$ [see Eq. (8)] for the dominant third-moment contribution vanishes identically. This implies a small value of

TABLE II. Parameters for the environmental repulsive term of BOP_0 and BOP.

	B (eV Å)	R_{core} (Å)	λ_0 ($Å^{-1}$)	C ($Å^{-m}$)	ν ($Å^{-1}$)	m	R_{tail} (Å)	R_{cut} (Å)
BOP	118.3	0.8	2.0	110.0	2.0	2.0	3.30	4.40
BOP_0	13.0	1.0	2.0	110.0	1.5	2.0	3.30	4.40

the screening function for $dd\sigma$ bond integrals at the second-nearest neighbor. On the other hand, $dd\pi$ and $dd\delta$ bonds are heavily screened at the second-nearest neighbors and both their magnitude and slope are reduced by a factor of 3.

The bond energy is dependent on the total number of d electrons. Molybdenum comprises six valence electrons that are distributed between the nearly free-electrons sp band and the tight-binding d band. The number of d electrons is usually noninteger due to hybridization and we used $N_d=4.2$ which is not too far from the value suggested by DFT-based calculations. However, it should be noted that the effect of sp-valent electrons is not ignored. Since nearly free electrons possess no angular character the sp-valence electrons are implicitly included both in the environment-dependent repulsion (reflecting their exclusion from the sizable ion core regions in transition metals) and in the pair potential (reflecting the attractive contributions from the s-d hybridization).

We have calculated the bond energy using the real-space order-N BOP method. In order to assure a reliable description of local bonding in defective regions and, in general, in less ordered environments, nine moments of the density of states are used in our calculations. This guarantees that all the important features of the density of states, in particular the bimodal behavior and pseudogap, are correctly reproduced. As explained in Sec. II, a fictitious temperature is introduced during the calculations to dampen the Friedel oscillations; similarly as in Ref. 37 it was chosen such that $k_BT=0.3$ eV.

The next step in the construction of BOP is fitting the purely repulsive environmentally dependent term U_{env} given by Eq. (10). As mentioned earlier, this term was originally introduced to remedy the problem of fitting negative Cauchy pressures exhibited by many intermetallic compounds.[39] However, even for materials with a positive Cauchy pressure, an exact fitting cannot usually be achieved without the environment-dependent repulsive term. E_{pair} cannot be used to reproduce the Cauchy pressures since its contribution is related to the contributions of the other parts of the cohesive energy via the equilibrium conditions,[37,62] and the bond part alone does not lead automatically to the correct Cauchy pressures. In the present case, U_{env} was fitted to reproduce $C_{12}-C_{44}$ which is the only Cauchy pressure in cubic structures. Since there are six adjustable parameters in the environmentally dependent term and only one fitted quantity, these parameters are far from unique. The dependence of the Cauchy pressure on parameters C, ν, m, and λ_0 is complicated and highly nonlinear. Values of these parameters were chosen such that the embedding exponential function in Eq. (11) decreases to zero between the second and third neighbors in the bcc lattice and the resulting value of λ was less than 10. The parameter R_c corresponds approximately to the radius of the core electrons. By varying the remaining parameter B, which controls the magnitude of the environmental contribution, we were then able to fit exactly the Cauchy pressure. It should be noted that in structures with more than one Cauchy pressure (e.g., noncubic compounds), fitting of the environmentally dependent term requires simultaneous variations of several parameters and the procedure becomes more involved.[39]

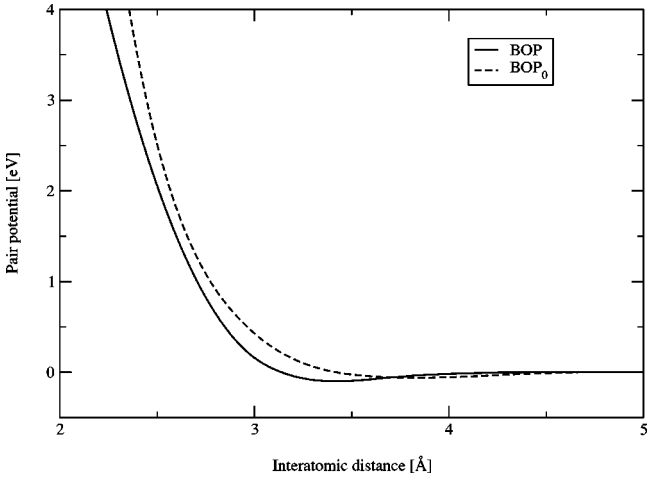

FIG. 3. Pair potential scaling for BOP and BOP_0 in Mo.

Similarly as in the case of the bond integrals, a smooth polynomial cutoff tail was introduced in the environmentally dependent term, namely for the embedding exponential function in Eq. (11). For $R_{tail}<R<R_{cut}$, this function is augmented by a polynomial of fifth order to ensure a smooth decay to zero. The final values of all the parameters of the environmental term are listed in Table II.

The pair potential [Eqs. (12) and (13)] is the last part of the cohesive energy to be fitted in the sequential procedure and ensures that the required ground-state structure is in equilibrium. It is principally repulsive but can also have an attractive region, as alluded to above. The quantities used to fit the pair potential are fundamental properties of the ground- state bcc structure, namely the cohesive energy, the lattice parameter, and remaining elastic moduli; one elastic

TABLE III. Fundamental properties of the ground-state bcc structure: lattice parameter a(Å), cohesive energy per atom (eV) (from Ref. 63) and elastic moduli (10^{11} Pa) (from Ref. 64).

a	U_{coh}	C_{11}	C_{12}	C_{44}
3.1472	6.82	4.647	1.615	1.089

TABLE IV. Parameters for the pair potentials for BOP_0 and BOP.

	BOP		BOP_0	
i	A_i (eV)	R_i (Å)	A_i (eV)	R_i (Å)
1	4.60	−0.078579421940	4.80	−0.319118706005
2	3.70	1.388283563938	4.60	0.507103162304
3	3.10	5.235057880439	3.60	0.979990469519
4	3.00	−5.990552025133	2.90	5.920419358904

modulus has been fixed by the Cauchy pressure via the environmental term. These empirical quantities are listed in Table III.

The chosen functional form of the pair potential [Eq. (13)] leads to the linear dependence of its contributions to the above four quantities on coefficients A_k. This is very convenient for the fitting since a set of linear equations then determines parameters A_k. The usual procedure adopted when fitting U_{pair} is to vary the node points R_k until a smooth and physically acceptable shape of the pair potential is attained. The values of the node points R_k and coefficients A_k that have been found using this procedure are summarized in Table IV and the resulting pair potential is displayed in Fig. 3.

In order to assess the importance of the screening of the bond integrals, we have also constructed a bond-order potential without the screening. In the following we designate it BOP_0 and the corresponding values of the parameters entering the generalized GSP function are summarized in Table V. The corresponding values of $\beta_\tau(R_0)$ are $dd\sigma_0 = -1.721$ eV, $dd\pi_0 = 0.792$ eV, and $dd\delta_0 = -0.096$ eV. Both the environmental part of the repulsion and the pair potential are, of course, different in this case and the corresponding parameters are summarized in Tables II and IV; the conforming pair potential is shown in Fig. 3.

IV. TESTING OF CONSTRUCTED POTENTIALS

In order to assess the reliability of constructed potentials we performed a variety of calculations the results of which can be compared either with *ab initio* calculations or experiments. Such testing is important for further studies of extended defects since the potentials were fitted to only a minimal number of empirical and *ab initio* data for the ground-state bcc structure and do not embody any implicit information about other nonequilibrium configurations. The attributes that have been computed are the energies of some alternate crystal structures, the variation of the energy with structural transformations that correspond to three distinct deformation paths, formation energies of vacancies and finally, the phonon-dispersion curves for the [100], [110], and [111] directions.

TABLE V. Parameters for GSP scaling function of BOP_0.

R_c (Å)	R_1 (Å)	R_{cut} (Å)	n_a	n_b	n_c
1.00	2.80	4.40	4.2	4.2	0.05

The first requirement for the validity of the constructed potentials is the stability of the ground-state bcc structure relative to alternative crystal structures. This has been tested by calculating energies of the A15, fcc, hcp, and simple cubic (sc) structures relaxed to their equilibrium densities. These calculations were performed using both the screened (BOP) and unscreened (BOP_0) potentials. The calculated energy differences between the alternative structures and the equilibrium bcc structure are summarized in Table VI where they can also be compared with calculations made by the DFT LMTO-ASA based method[45] and an environment-dependent spd tight-binding scheme using k space that was applied to studies of defects.[45] These results show that not only is the bcc structure most stable but that BOP reproduces well most structural energy differences found by DFT and is superior to BOP_0. However, the energy of the A15 structure predicted by BOP deviates from *ab initio* results appreciably. We believe that this is related to our neglect of the nonorthogonality screening function in the repulsive potential.

Since the potentials are intended for atomistic modeling of extended defects, they have to be applicable when the atomic environment is considerably different from that in the ideal lattice. While this can never be fully tested, investigating the highly distorted structures encountered along certain transformation paths can provide a meritorious assessment of the potentials. Three such paths, tetragonal, trigonal, and hexagonal[65] have been investigated. The energy was calculated as a function of parameters characterizing these paths using both BOP and BOP_0 and compared with the analogous calculations made by the *ab initio* FLAPW method.[66,67]

The most common transformation path is the tetragonal path, also known as the Bain path,[68] between the bcc and fcc lattices. It is a deformation path along which the body-centered tetragonal (bct) structure is stretched along the [001] axis and the high-symmetry bcc and fcc structures are

TABLE VI. Comparison of the energies (ev/atom) relative to bcc of four structures calculated using BOP, BOP_0, a DFT-based method, and an environment-dependent tight-binding (EDTB) method.

	DFT	BOP	BOP_0	EDTB
A15	81	457	228	173
fcc	460	478	427	520
hcp	490	494	446	550
sc	768	767	1193	723

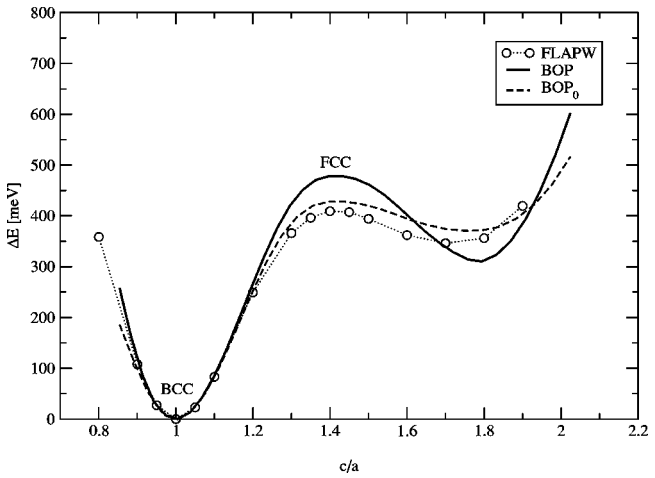

FIG. 4. Energy per atom, relative to the energy of the bcc lattice, as a function of c/a for the tetragonal deformation path calculated by BOP, BOP_0, and FLAPW.

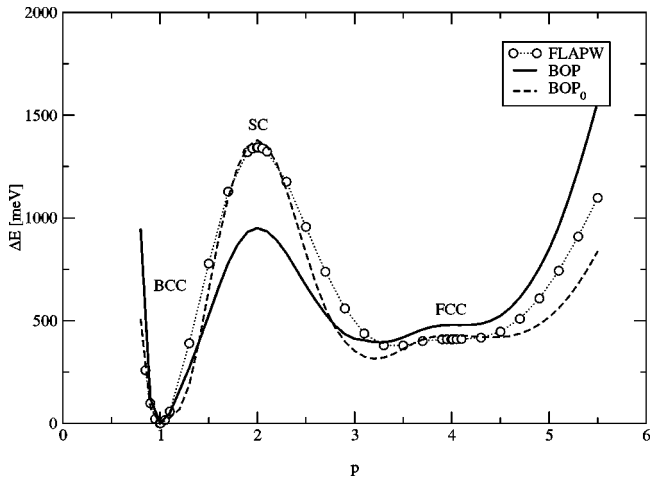

FIG. 5. Energy per atom, relative to the energy of the bcc lattice, as a function of the parameter p for the trigonal deformation path calculated by BOP, BOP_0, and FLAPW.

obtained as special cases. The bct structure can be parametrized in terms of the c/a ratio (where a is the lattice parameter in the [100] and [010] directions and c in the [001] direction), with $c/a=1$ corresponding to the bcc structure and $c/a=\sqrt{2}$ to the fcc structure. The volume per atom is constant for all structures along this path. Comparison of our calculations with *ab initio* results is shown in Fig. 4.

The second transformation path we investigated is the trigonal path, which is also a deformation path between the bcc and fcc lattices but passing through the sc structure. Starting from the bcc lattice, the trigonal path concurs with the homogeneous deformation corresponding to the extension along the [111] axis while keeping the atomic volume constant. In the coordinate system with the x, y, and z axes parallel to $[1\bar{1}0]$, $[11\bar{2}]$, and [111] directions it is described by the following Lagrangian strain tensor for large deformations:

$$\varepsilon_{11}=\varepsilon_{22}=(p^{-2/3}-1)/2,$$

$$\varepsilon_{33}=(p^{4/3}-1)/2,$$

$$\varepsilon_{12}=\varepsilon_{13}=\varepsilon_{23}=0, \tag{15}$$

where p is a parameter characterizing the deformation; it varies from 1 for bcc, through 2 for sc to 4 for fcc lattices. The magnitude of the vectors parallel to $[1\bar{1}0]$ and $[11\bar{2}]$ directions is proportional to $p^{-1/3}$ while the magnitude of the vectors parallel to the [111] directions is proportional to $p^{2/3}$. The calculated dependence of the energy per atom on the parameter is shown in Fig. 5. It should be noted that the extrema for $p=1$, 2, and 4, corresponding to different cubic structures, are dictated by the symmetry. However, the presence of auxiliary minima in the vicinity of $p=4$ is specific to the material studied.

The last investigated path is the hexagonal transformation path. This connects the bcc and hcp lattices and it differs qualitatively from the other two paths since it does not correspond to a homogeneous straining. Instead, it is a combination of a homogeneous deformation that preserves the atomic volume, with shuffling of alternate close-packed atomic planes in opposite directions. Starting with the bcc lattice, the part corresponding to the homogeneous deformation is described in the coordinate system with x, y, and z axes parallel to $[1\bar{1}0]$, [001], and [110] directions, respectively, by the Lagrangian strain tensor of finite deformations:

$$\varepsilon_{11}=\{[1+\alpha_1(1-p)]^2-1\}/2,$$

$$\varepsilon_{22}=\{[1+\alpha_1(1-p)]^2-1\}/2,$$

$$\varepsilon_{33}=([\beta_0+\beta_1 p+\beta_2 p^2]^{-2}-1)/2, \tag{16}$$

where

$$\alpha_1=\frac{1-2^{-1/6}\sqrt{1.5}}{\sqrt{2}-1}\approx -0.2200,$$

$$\alpha_2=\frac{1-2^{-1/6}}{\sqrt{2}-1}\approx 0.2956,$$

$$\beta_0=\alpha_1\alpha_2+\alpha_1+\alpha_2+1,$$

$$\beta_1=-2\alpha_1\alpha_2-\alpha_1-\alpha_2,$$

$$\beta_2=\alpha_1\alpha_2. \tag{17}$$

For this transformation, the magnitudes of the vectors parallel to $[1\bar{1}0]$ are proportional to $1+\alpha_1(1-p)$, vectors parallel to [001] to $1+\alpha_2(1-p)$, and vectors parallel to [110] are determined such that the volume is conserved. However, together with this straining, alternate (110) planes are displaced for each value of p in the directions $\pm[110]$ by $a_0 2^{-1/6}(p-1)/[2\sqrt{3}(\sqrt{2}-1)]$. Thus, we interpolate linearly between the bcc and hcp structures in the directions $[1\bar{1}0]$ and [001] and the shuffling is linearly coupled to the magnitude of straining in these directions. $p=1$ corresponds

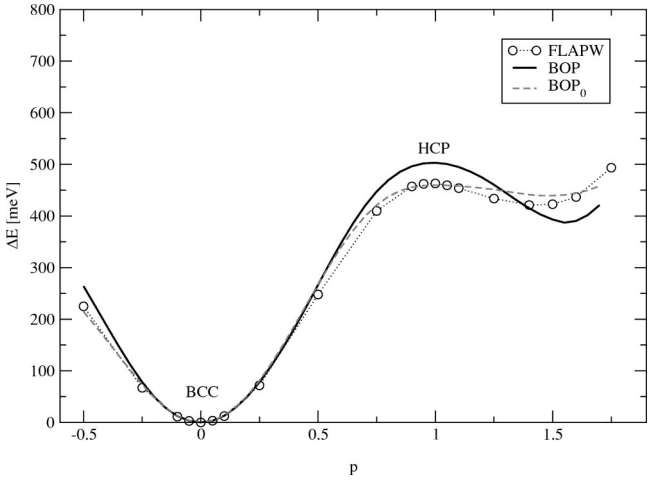

FIG. 6. Energy per atom, relative to the energy of the bcc lattice, as a function of the parameter p for the hexagonal deformation path calculated by BOP, BOP_0, and FLAPW.

to the bcc lattice and $p=\sqrt{2}$ to the hcp lattice. The results of calculations for the hexagonal path are displayed in Fig. 6.

In general, both BOP and BOP_0 reproduce the *ab initio* data closely and are able to trace correctly even certain subtle features that originate from the directional character of bonding. An example is the occurrence of two energy minima in the vicinity of the fcc structure along the trigonal path; for the fcc structure the energy then reaches a local maximum. All these features of the trigonal deformation path are correctly reproduced by our potentials. We should emphasize here that in contrast to our model, the central-force potentials (e.g., Finnis-Sinclair many-body potentials) give only one local minimum for the trigonal path, corresponding to the fcc structure.[52]

Another test that probes the applicability of potentials in a locally disordered environment is study of a vacancy. This crystal defect was modeled using periodic boundary conditions in all directions with the repeat cell of the size $3a \times 3a \times 3a$, where a is the lattice parameter, containing a total of 53 atoms. The atomic configuration was fully relaxed under the condition of constant volume. The vacancy formation energy is defined as

$$U^f = U_{tot}[N] - N\,U_{coh}, \tag{18}$$

where U_{tot} is the total energy of the simulated system, N the number of atoms in the simulation cell with the vacancy, and U_{coh} the cohesive energy per atom in the bulk. The vacancy formation energies calculated using both BOP and BOP_0 are 3.5 eV and 2.3 eV, respectively. The formation energy obtained using the BOP compares very well with *ab initio* results and experimental data (from Refs. 69–72 and references therein) that lie in the range 2.9–3.2 eV. The formation energy predicted by BOP_0 is rather low which again demonstrates the importance of screening.

The final thorough test of the potentials is a comparison of calculated phonon-dispersion curves with experimental data. The phonon spectra were computed for three high-symmetry directions using the method of frozen phonons.[73] The more general evaluation of the phonon spectrum that requires determination of the dynamical matrix is rather complicated in the BOP scheme since the computation of the second derivatives of the bond part is not a trivial task. In principle, it is possible to obtain the dynamical matrix numerically but such calculations require large supercells so that the long-range couplings, present in transition metals, are correctly accounted for. In frozen phonon calculations all conceivable couplings between the atoms are accounted for exactly and thus this calculation provides reliable phonon frequencies even with small simulation blocks.

We performed the frozen phonon calculations for several displacements in the range $\pm 0.02a$, for which we assume that the harmonic approximation holds. The phonon frequencies were then computed by fitting the energy versus displacement data by a polynomial of second order using the least-squares method. The results for both BOP and BOP_0 are presented in Fig. 7 together with experimental data from inelastic neutron-scattering measurements[74] for comparison.

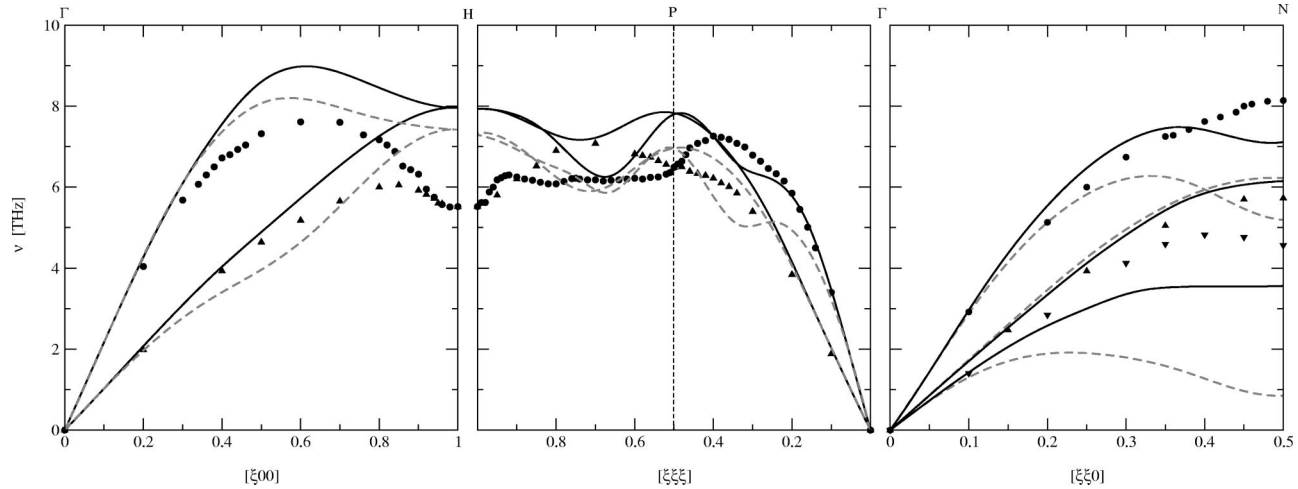

FIG. 7. Phonon-dispersion curves for three high-symmetry directions. Dashed and full curves represent results calculated by BOP_0 and BOP, respectively; symbols show experimental data (Ref. 74).

TABLE VII. Values of force constants for the first-, α_1, and second-, β_2, nearest neighbors, respectively, for Mo within both BOP_0 and BOP (in N/m).

	BOP_0	BOP
α_1	13.9	19.8
β_2	−15.8	−8.4

Despite some minor quantitative discrepancies, the agreement is satisfactory for the [100] and [111] directions and both potentials. However, the longitudinal- (L) mode and transverse- (T2) mode (polarization along [001]) phonons at the zone edge in the [110] direction, predicted by unscreened BOP_0, are much softer than experiments suggest. When using the nonorthogonal screened potential (BOP) the frequency of the T2 *N*-phonon mode increases more than threefold. Changes of the remaining two modes, while not so dramatic, also lead to dispersion curves that are closer to the experimental ones.

The problem of too soft *N*-point phonons in Mo and W is common in semiempirical TB schemes. It is therefore desirable to ascertain the underlying physical reason for the large improvement when the screening of bond integrals has been introduced. As mentioned earlier, in the case of BOP_0 the second-nearest-neighbor $dd\pi$ and $dd\delta$ bond integrals are not represented with sufficient precision by simple scaling functions owing to the evident discontinuity between first- and second-nearest neighbors. This is critical for the values of the second-nearest neighbor force constants which then strongly influence the phonon spectra. Indeed, it was shown by Foiles[69] that it is the fourth moment of the density of states, i.e., the moment which links the second-nearest neighbors, that affects the behavior of phonons in the [110] direction most profoundly. Hence, when the screening concept is introduced and the $dd\pi$ and $dd\delta$ bond integrals are reproduced with much higher precision, the accuracy of the phonon spectra improves significantly.

In order to elucidate further the origin of this improvement, we have investigated various contributions to the force constants and their differences between the BOP_0 and BOP schemes. The frequency of each phonon mode can be written as a linear combination of certain force constants.[75] The coefficients in these linear combinations of force constants are functions of the particular direction and branch under consideration. The frequency of the T2 *N*-point phonon in the bcc crystal, when interatomic interactions up to the fifth-nearest neighbors are considered, is given as[76]

$$[110]T2: \quad 4\pi^2 M\nu^2 = 8\alpha_1 + 8\beta_2 + 16\alpha_3 + 8\alpha_4 + 16\beta_4, \tag{19}$$

where α_n and β_n are interatomic force constants for different vibrational modes of the nth neighbor.

We have calculated numerically the first- and second-nearest-neighbor force constants α_1 and β_2 which give the biggest contributions and thus are sufficient for explanation of the differences in the phonon behavior. Values of these force constants, calculated by both BOP_0 and BOP, are presented in Table VII. Both α_1 and β_2 increase significantly when screening is applied. For orthogonal unscreened BOP_0, the sum of these two terms is negative. This means that in the approximation of first- and second-nearest neighbors the phonon frequency is imaginary and the T2 *N*-point phonon is only stabilized by the terms corresponding to more distant neighbors in Eq. (19). When nonorthogonal screening is applied, $\alpha_1 > |\beta_2|$ and, therefore, already the first- and second-nearest-neighbor interactions yield not only real value of the phonon frequency but also its much larger magnitude.

However, it should be noted that these changes are not solely due to the screened bond integrals that directly affect the bond part of the energy but result from both the bond and repulsive parts of the potential. Nonetheless, since the repulsive part has been fitted only after the bond part contributions have been fixed, it is, indeed, the more accurate description of bond integrals that is the primary reason for the improved phonon behavior. This conclusion is further supported by the fact that modifications of the repulsive terms in the nonorthogonal unscreened BOP_0 did not lead to any improvements in the phonon spectra.

V. STRUCTURE AND GLIDE OF SCREW DISLOCATIONS IN MOLYBDENUM

It has already been mentioned in the Introduction that distinguishing features of the plastic behavior of bcc metals are controlled by the structure and properties of the dislocation cores. As first suggested by Hirsch[77] and now firmly established by many experimental and theoretical studies (for reviews see Refs. 4–8), dislocations controlling the characteristic features of the plastic properties of bcc metals are $1/2\langle 111\rangle$ screw dislocations. The most general reason is crystallographic: $\langle 111\rangle$ is the direction of a threefold screw axis in the bcc lattice and thus the structure of the dislocation parallel to this direction must possess such symmetry and is, therefore, intrinsically nonplanar.[78] This further suggests that screw dislocations will be more difficult to move than dislocations of other orientations. However, crystallography alone does not determine into which planes of the $\langle 111\rangle$ zone and in what manner the core is spread in space and, even more importantly, how such core responds to external loading. Capability to observe the atomic structure of the core directly is very limited[79] and a direct observation of the stress effects is not even feasible. Consequently, investigation of this phenomenon is an excellent topic for atomistic simulation and we present such study using the constructed BOP.

Notwithstanding, this is not the first study of this type; a large number of simulations of dislocations in bcc metals have been made using a broad variety of descriptions of atomic interactions (for reviews see Refs. 7 and 80). In these studies the core was always found to spread into three {110} planes, specifically $(\bar{1}01)$, $(0\bar{1}1)$, and $(\bar{1}10)$ for the $1/2[111]$ dislocation [see Fig. 9(b)]. Still, two types of the core were uncovered that differ in invariance with respect to another symmetry operation of the bcc lattice, the $[10\bar{1}]$ diad. In one case the core is spread asymmetrically into these three planes and is not invariant with respect to this symmetry operation while in the other case it is invariant, spread

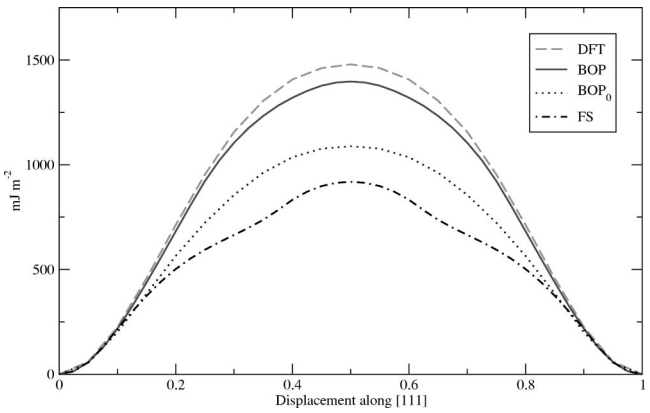

FIG. 8. [111] cross sections of the γ surface for the plane in molybdenum calculated using the Finnis-Sinclair- (FS) type central-force many-body potentials (Ref. 25), BOP_0, BOP, and an *ab initio* DFT method.[86] Displacement is normalized by the magnitude of the 1/2[111] vector.

symmetrically. In the former case two configurations related by the $[10\bar{1}]$ diad exist and thus this core is called degenerate and the latter one nondegenerate. In the [111] projection, which is usually used when depicting the core, the former structure appears as threefold and the latter as sixfold. Which of the core structures is found depends on the description of atomic interactions used in the calculations and thus material but both types have been found for nominally the same metal when using different descriptions of atomic interactions. Taking as example molybdenum, recent calculations[26,27] employing many-body central-force potentials of the Finnis-Sinclair type,[25] as well as calculations[70,81] employing potentials derived from generalized pseudopotential theory,[31,32] showed the degenerate core. In contrast, the nondegenerate structure was found in some earlier tight-binding calculations[82,83] and the most recent *ab initio* DFT-based calculations.[29,51,84] The latter give us again an opportunity to compare BOP and *ab initio* calculations and thus further assess the quality of BOP.

A. γ surfaces

It is always profitable to investigate first γ surfaces for the planes into which the dislocation may be spreading before any study of the dislocation core structure.[2,3,80] This theoretical construct represents the energy of a ''generalized'' stacking fault, formed by displacing the two parts of the crystal relative to each other along a crystal plane, as a function of this displacement. When calculating the γ surface, relaxation perpendicular to the plane of the fault but not parallel to this plane is carried out since the latter would eliminate the generalized stacking fault. Minima on such surface determine possible metastable stacking faults that can participate in dislocation dissociation into partials which is the most important core effect. Indeed, this concept was originally introduced when searching for possible stacking faults in bcc metals.[85] Moreover, it was shown by Duesbery and Vitek[26] that by analyzing the γ surfaces for {110} planes it can be predicted whether the core of the screw dislocation is degenerate or nondegenerate. This is demonstrated below.

Using BOP the γ surfaces were calculated for both {110} and {112} planes. Their overall profiles are the same as those found in many previous calculations (see, e.g., Ref. 80) and they are not, therefore, presented here. In both cases there are no local minima which would correspond to metastable stacking faults on these planes and, indeed, no splitting of dislocations in bcc metals has ever been observed and it is generally accepted that in these materials such faults do not exist.[6] The [111] cross section of the γ surface for the $(\bar{1}01)$ plane is shown in Fig. 8. Besides the calculation employing the BOP we also present calculation made using BOP_0, the central-force many-body potentials of the Finnis-Sinclair type,[25] and results of a recent *ab initio* DFT-based calculation.[86] An excellent agreement between the *ab initio* and BOP results is obvious while it is appreciably worse for BOP_0 and poor for central-force many-body potentials.

As seen in Fig. 8, for displacements smaller than $0.15b$, where b is the magnitude of the 1/2[111] vector, all four cross sections of the γ surface are virtually identical. The

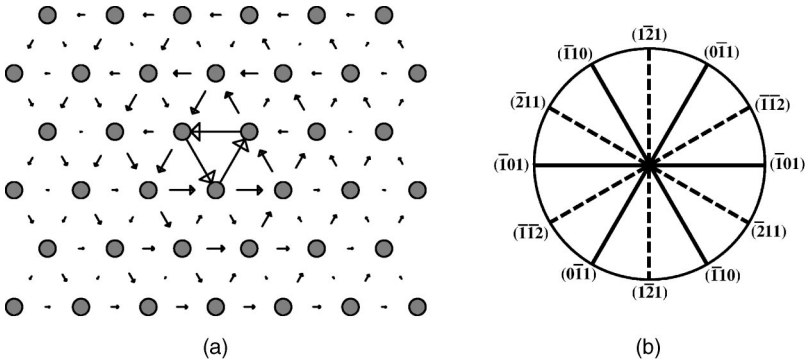

FIG. 9. (a) Core structure of the 1/2[111] screw dislocation determined using BOP for molybdenum. The atomic arrangement is shown in the projection perpendicular to the direction of the dislocation line ([111]) and circles represent atoms within one period, without distinguishing their positions in three successive (111) planes. The [111] (screw) component of the relative displacement of the neighboring atoms produced by the dislocation is depicted as an arrow between them. The length of the arrows is proportional to the magnitude of these components. The arrows, which indicate out-of-plane displacements, are always drawn along the line connecting neighboring atoms and their length is normalized such that it is equal to the separation of these atoms in the projection when the magnitude of their relative displacement is equal to $|1/6[111]|$. (b) [111] stereographic projection showing orientations of all {110} and {112} planes belonging to the [111] zone.

reason is that this is the harmonic regime and both the BOP and the central-force potential were fitted to the elastic moduli of molybdenum that are also well reproduced in the *ab initio* calculations. However, for larger displacements the γ surfaces evaluated *ab initio* and using the BOP attain appreciably higher values. For these displacements both the separations of atoms on each side of the corresponding generalized stacking fault and the bond angles are very different from those in the ideal bcc lattice. When calculating the γ surface only relaxation perpendicular to the plane of the fault is allowed. This relaxation may alter significantly the separations of atoms. In particular, it will eliminate any configuration in which the atoms would be at a distance appreciably smaller than the spacing of the nearest neighbors when their repulsion would be very strong. However, this relaxation will affect much less the bond angles. The dependence of the energy on these angles is included most precisely in the BOP, with a lower precision in BOP_0, while only the separation of atoms enters for the central-force potentials. Figure 8 clearly shows that the agreement with *ab initio* calculations is the better the more accurately the dependence of the energy on bond angles is described. Hence, it must be the angular dependence of the interatomic interactions, best captured by BOP, that is responsible for high values of the γ surface at large displacements.

B. Core structure

The computer modeling of the core structure using BOP was performed employing the same procedure as in earlier calculations with central forces.[26,27] Periodic boundary conditions were imposed parallel to the dislocation line while perpendicular to the dislocation the block consisted of an active region in which all the atoms were fully relaxed and an inactive region where the atoms are permanently displaced in accordance with the anisotropic elastic field of the dislocation.[87] The active, fully relaxed region contained 720 atoms and the inactive region 860 atoms; in the latter no relaxation is allowed but the atoms interact with those in the active region. The result of this study is shown in Fig. 9(a) using the usual differential displacement map, defined in the captions of this figure; Fig. 9(b) shows orientations of all $\{110\}$ and $\{112\}$ planes belonging to the $[111]$ zone. The core is obviously nondegenerate, spread symmetrically into the three $\{110\}$ planes. This is in contrast with the degenerate core found in calculations using central-force potentials for molybdenum[3,26–28,80] but in complete agreement with recent *ab initio* calculations[29] that employed flexible boundary conditions which couple self-consistently the long-range elastic strain field with the strain field near the core, eliminating any possible influence of the block size on the calculated core structure.[51]

Following Ref. 26, which of the two core structures is found can be rationalized with the help of the γ surface for $\{101\}$ planes. The degenerate core comprises three faults corresponding to the displacement $\boldsymbol{b}/3$, where $\boldsymbol{b}$ is the $1/2[111]$ Burgers vector, on $(\bar{1}01)$, $(1\bar{1}0)$, and $(01\bar{1})$ planes and the nondegenerate core six faults with the displacement $\boldsymbol{b}/6$ on the same planes. Hence, the energy difference between the two cores can be approximately assessed as follows: The degenerate core will be favored if $3\gamma(\boldsymbol{b}/3) < 6\gamma(\boldsymbol{b}/6)$ and vice versa for the nondegenerate core. Based on the results shown in Fig. 8, $3\gamma(\boldsymbol{b}/3)$ equals 2133 $\mathrm{mJ\,m^{-2}}$ for the Finnis-Sinclair type potentials and 3579 $\mathrm{mJ\,m^{-2}}$ for the BOP and $6\gamma(\boldsymbol{b}/6)$ equals 2508 $\mathrm{mJ\,m^{-2}}$ and 3090 $\mathrm{mJ\,m^{-2}}$, for these two potentials, respectively. This implies that for molybdenum the degenerate core should be favored when using the Finnis-Sinclair-type potentials and the nondegenerate core for the BOP. Indeed, this is what the computer modeling of the core structure shows. It is argued above that it is the angular dependence of the interatomic interactions, captured in the BOP scheme, that is responsible for higher values of the γ surface than for central forces and consequently, the nondegenerate core structure in molybdenum presumably results from the angular character of bonding. Since *d* electrons dominate cohesion in transitions metals, the directional character of bonding is generally important and thus the nondegenerate cores are likely to be more common than the degenerate ones in these metals.

C. Effect of externally applied stress

The ultimate goal of studies of dislocations is understanding their glide behavior under external loading. Detailed atomistic studies of the effect of stress fields encountered in real situations are in progress and will be published elsewhere. Here we only present a study of the effect of the pure shear stress acting in the direction of the Burgers vector with various orientations of the maximum resolved shear stress plane (MRSSP). The goal is to investigate the dependence of the stress at which the dislocation starts to move on this orientation. A similar study, albeit limited to only three orientations of the MRSSP, was recently made using an *ab initio* DFT-based method[51] and this provides another opportunity for comparison between BOP and *ab initio* calculations.

The orientation of a MRSSP is defined by the angle χ which this plane makes with the $(\bar{1}01)$ plane. Owing to the crystal symmetry it is sufficient to consider $-30° < \chi < +30°$; for $-30°$ the MRSSP is the $(\bar{1}\bar{1}2)$ plane and for $+30°$ the $(\bar{2}11)$ plane but note that orientations corresponding to positive and negative angles χ are not equivalent. In the following, we always give the shear stress acting in the $[111]$ direction as the stress in the MRSSP, and its value when the dislocation starts to move is identified with the critical resolved shear stress (CRSS) for the dislocation glide at 0 K. When applying the stress the elastic displacement field corresponding to this stress was evaluated using anisotropic elasticity and superimposed on the dislocation displacement field for the atoms in both the active and inactive regions. The relaxation then proceeded as in the nonstressed case. The calculation always started with the fully relaxed core structure and the applied stress was built up incrementally and full relaxation carried out at every step until the dislocation started to move. This stress level was then identified with the CRSS.

Upon reaching the CRSS the dislocation moved along the $(\bar{1}01)$ plane for all angles χ. The calculated dependence of the CRSS on χ is displayed in Fig. 10 where data from *ab*

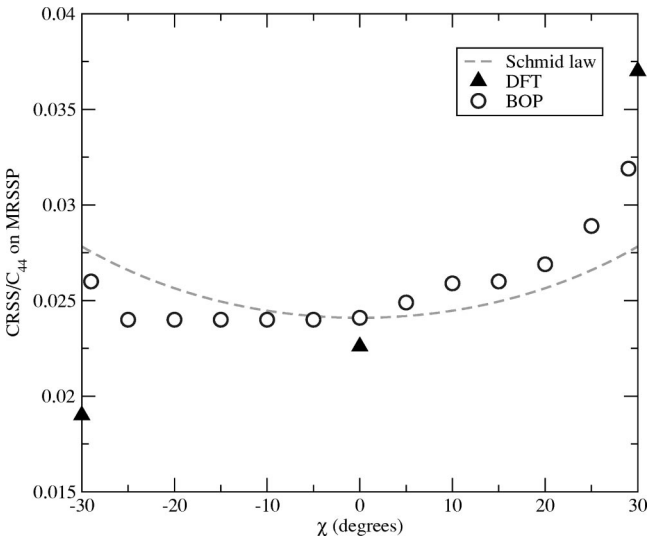

FIG. 10. Dependence of the CRSS on the angle χ in molybdenum calculated using BOP (circles) and by an *ab initio* method based on the DFT (triangles) (Ref. 51).

initio calculations[51] for $\chi=0°$ and $\chi=\pm 30°$ are also shown. The agreement between BOP and *ab initio* calculations is excellent for $\chi=0°$ but less satisfactory for χ close to $\pm 30°$. A possible reason for the lesser agreement for $\pm 30°$ is that in this case the shear stress is exactly the same in two different $\{101\}$ planes, e.g., $(\bar{1}01)$ and $(01\bar{1})$, and thus the glide plane is not uniquely defined. This may affect in an ill-defined way the values of the CRSS calculated for $\chi=\pm 30°$. For this reason our calculations were not made for these bordering angles but for angles χ differing by about $2°$ from $\pm 30°$. However, most importantly, both BOP and *ab initio* calculations exhibit the same asymmetry in the orientation dependence of the CRSS, in particular higher CRSS for $\chi>0$, i.e., antitwinning sense of shearing and lower CRSS for $\chi<0$, i.e., twinning sense of shearing.

As seen from Fig. 10, the CRSS does not obey the Schmid law according to which the dependence of the CRSS on χ should have the form $1/\cos\chi$, shown by the solid curve in this figure. It is larger for positive than for negative angles χ, which is related to the so-called twinning-antitwinning asymmetry.[6] For negative χ the nearest $\{112\}$ plane, $(\bar{1}\bar{1}2)$, is sheared in the twinning sense, i.e., such that a twin would be formed if such shears were made in successive $(\bar{1}\bar{1}2)$ planes. For positive χ the nearest $\{112\}$ plane, $(\bar{2}11)$, is sheared in the antitwinning sense. In the bcc lattice there is, of course, no crystallographic reason why shearing in opposite directions along $[111]$, which is commensurate with changing the sign of the angle χ, should be equivalent. The reason is that $\{111\}$ planes are not mirror planes in this lattice. However, symmetry arguments cannot predict whether the CRSS will be larger for positive than for negative χ or vice versa. Both the BOP and *ab initio* calculations predict the former, which is in good agreement with experimental observations.[4–8]

VI. DISCUSSION AND CONCLUSIONS

In this paper we have developed, tested, and employed to a study of the core structure and glide of screw dislocations, the screened bond-order potentials for molybdenum. This real-space description of interactions between the atoms, which is based on the parametrized tight-binding approximation to the electronic structure, is capable of treating mixed metallic and covalent bonding common in transition metals and their alloys. This is crucial for atomic-level modeling of extended defects in these materials since the angular character of bonding may govern both their structures and properties. This angular dependence results from the directional character of *d* orbitals and enters the attractive bond energy contribution in BOP. In contrast, the repulsive part of the energy has a central-force nature and relates to the metallic character of the bonding. The distinguishing feature of the constructed BOP is that both the bond energy and the repulsive contribution to the cohesive energy comprise environmental dependencies. The importance of these dependencies has been demonstrated in both testing and application of the potentials and will be discussed further below.

In the present development the bond energy has been evaluated within the *d*-band model, the justification of which is discussed in Sec. III, and thus only $dd\sigma$, $dd\pi$, and $dd\delta$ bond integrals are needed. Following Slater and Koster,[40] the intersite Hamiltonian matrix elements can be separated into radial and spherical parts characterizing the angular variation of the bond orbitals. The scaling of the radial part has been represented analytically according to Eq. (5). However, an additional angular dependence arises owing to the environmental dependence of the bond integrals which is here described as screening of the *d*-*d* bonds by *s*-valence electrons associated with atoms neighboring a given bond. The angular character of the orbitals forming the bond that is being screened plays a key role in the ensuing environmental dependence of bond integrals. The corresponding angularly dependent screening function, which has been derived analytically within a nonorthogonal TB representation using the bond-order formalism,[47] contains only five adjustable parameters related principally to the appropriate overlap integrals. Critically, in contrast to previous schemes,[45] this screening function contains explicit angular dependence reflecting the directional character of the σ, π, and δ bond integrals that are being screened.

The most remarkable ability of the analytic screening function is its capacity to reproduce conspicuous discontinuities between the first- and second-nearest neighbors in bond integrals found in *ab initio* calculations (see Fig. 1). These arise because the environment of the first- and second-nearest neighbors is not the same and the screening function, owing to its angular dependence, reflects this difference correctly. This clearly demonstrates that the environment-dependent screening of the bond integrals enhances greatly our ability to mimic in the BOP scheme the bond integrals found in *ab initio* calculations and thus capture the environmental effects in atomic-level calculations employing BOP.

Furthermore, another environmental dependence appears in the repulsive, central-force part of the binding energy. As

explained in Sec. II, this part consists of pair and many-body contributions. The latter results from the repulsion of the valence *s* and *p* electrons as they are squeezed into the ion core regions under the influence of the large covalent bonding forces[56] and is environmentally dependent. This part of the repulsion is essential for correct reproduction of elastic moduli within the BOP scheme. Specifically, it allows for exact fitting of the Cauchy pressure that is not affected by the pair contribution[57,62] and would otherwise be determined by the bond energy only.[37] This is of paramount importance for materials with negative Cauchy pressures, such as iridium and many intermetallic compounds (e.g., TiAl and $MoSi_2$). However, as discussed in Sec. III, without the environmentally dependent repulsion the Cauchy pressure could not be reproduced even in molybdenum although it is positive.

When testing the constructed potentials the effect of screening is most dramatic for the case of Γ-*N* branch of the phonon spectrum. In the case of BOP_0 the L and T2 phonons are appreciably softer than experiments suggest. This is most pronounced close to the *N* point. Indeed, the analysis of the force constants, presented in Sec. IV, shows that for the T2 *N*-point phonon the frequency would be imaginary if only interactions of the first and second neighbors were taken into account and it is real only owing to interactions of more distant neighbors. However, in the case of BOP the same analysis shows that the frequency of T2 *N*-point phonon is real even when only first- and second-neighbor interactions are considered. As seen in Fig. 7, for BOP the frequency of the T2 *N*-phonon is more than three times higher than for BOP_0 and, in general, the phonon-dispersion curves for the Γ-*N* branch are much closer to the experimental ones. The environmental dependence of the bond integrals appears to solve the problem of too soft *N*-point phonons in Mo. This is very significant for atomistic modeling of extended crystal defects. Low, or in the worst case imaginary, phonon frequencies may affect such simulations significantly and physically incorrectly if similar displacements occur within these defects. The lattice may deform too easily in the directions of soft phonons and this might induce unphysical relaxations and even structural transformations. This danger is obviously much smaller in the case of BOP than for BOP_0.

Another important test is investigation of transformation paths along which the structures that deviate very significantly from the bcc lattice are encountered. Three such paths, tetragonal, trigonal, and hexagonal, were investigated by calculating the energies of the structures met along these paths using the constructed potentials and comparing the results with those obtained in analogous *ab initio* calculations. Both BOP_0 and BOP reproduce the *ab initio* data well and thus this analysis does not reveal any critical impact of the screening of the bond integrals. Nevertheless, these calculations do highlight the importance of directional bonding in modeling structures that differ considerably from the ideal bcc lattice. The bond-order potentials are capable to capture subtle features, such as two energy minima in the vicinity of the fcc structure along the trigonal path (see Fig. 5), that apparently result from the directional character of bonding as they are not reproduced when using central-force potentials.[52]

Clearly, an imperative requirement is that the constructed potentials assure that the bcc structure is the most stable when compared with alternative crystal structures. This has been tested by calculating energies of several such structures (A15, fcc, hcp, and simple cubic). Indeed, both the BOP_0 and BOP favor the bcc structure by a large margin. Furthermore, BOP reproduces the structural energy differences found by *ab initio* calculations closely and is obviously preferred over BOP_0.

The test of both validity and applicability of the constructed potentials is the modeling of the core structure and glide of the $1/2\langle 111\rangle$ screw dislocations, which is the dislocation controlling the characteristic features of the plastic deformation of bcc metals. The helpful precursor of the study of dislocation cores is calculation of the γ surfaces for planes into which the core may be spreading. In the bcc lattice these are $\{110\}$ and $\{112\}$ planes. While the profiles of the γ surfaces calculated using BOP, BOP_0, and the central-force Finnis-Sinclair-type potentials are not principally different, only the γ surface calculated using the BOP is in absolute values very close to that calculated *ab initio*.[86] As explained in Sec. V, the reason is that in the BOP scheme the dependence of the energy on bond angles is covered most precisely. This is, presumably, also the reason why the vacancy formation energy predicted by BOP_0 is appreciably lower than that found using BOP that is then in the range of experimental values as well as formation energies calculated *ab initio*.

The core structure of the $1/2\langle 111\rangle$ screw dislocation calculated using BOP agrees excellently with that found in the recent *ab initio* calculations.[29] The core is nondegenerate and is invariant with respect to the threefold screw symmetry of the $[111]$ axis as well as with respect to the $[10\bar{1}]$ diad. This is in contrast with many previous studies that suggested a degenerate structure not invariant with respect to the $[10\bar{1}]$ diad; two configurations related by this symmetry operation then exist. As proposed in Ref. 26 and discussed in Sec. V, the type of the core structure and the magnitude of the γ surface are related. Specifically, if $3\gamma(\boldsymbol{b}/3) > 6\gamma(\boldsymbol{b}/6)$ for the $\{101\}$ γ surface, the nondegenerate core is favored and vice versa for the degenerate core. Hence, since the $\{110\}$ γ surfaces calculated by the BOP and *ab initio* are virtually identical, it is not surprising that the same core structure has been obtained in both calculations. In contrast, in the case of the Finnis-Sinclair-type potentials the above criterion predicts the degenerate configuration which has, indeed, been found.[26,27,80] For the γ surface calculated using the BOP_0 $3\gamma(\boldsymbol{b}/3)$ equals 2780 mJ m^{-2} and $6\gamma(\boldsymbol{b}/6)$ 2665 mJ m^{-2} so that they differ only by 4%. In this case the above criterion is too nebulous to differentiate between the two competing core structures. The limited calculations using the BOP_0 suggest that in this case the core of the $1/2\langle 111\rangle$ screw dislocation is degenerate but so narrowly spread into the $(\bar{1}01)$, $(1\bar{1}0)$, and $(01\bar{1})$ planes that it is hardly distinguishable from the nondegenerate one.

Finally, the modeling of the glide of the screw dislocation under the effect of applied shear stresses parallel to the Burgers vector again shows a very good agreement with available *ab initio* calculations, both in absolute values of the

shear stress at which the glide commences (CRSS) and in the form of the dependence of the CRSS on the orientation of the MRSSP. Specifically, the CRSS is higher for those orientations for which the nearest {112} plane is sheared in the antitwinning sense than for orientations for which the nearest {112} plane is sheared in the twinning sense. This is in agreement with many experimental observations[4–8] and it is the primary reason for the breakdown of the Schmid law. This and other asymmetries of the dislocation motion that are a consequence of the atomic structure of screw dislocation core may play a very important role in the macroscopic plastic behavior of bcc transition metals, including properties of polycrystals.[88] These aspects of yielding need to be incorporated into the corresponding constitutive equations so that the atomic-level understanding of dislocation behavior is transferred to nanoscale and ultimately to macroscopic level. This goal can only be achieved via reliable atomic-level modeling of the motion of dislocations.

Considering both the extensive testing and very successful application, we can conclude that the bond-order potential for molybdenum that includes screening of the bond integrals, developed in this study, is eminently suitable for atomistic studies of crystal defects in transition metals. It not only guarantees the stability of the bcc structure for group V and VI transition metals and reproduces a number of equilibrium properties as do many other descriptions of atomic interactions, but reflects accurately the very important feature of mixed metallic and covalent bonding, the dependence of the cohesive energy on bond angles arising due to the partially filled *d* band. Furthermore, it is adequately transferable to structures that deviate very significantly from the ideal lattice. Hence, the potential is likely to reveal correctly the structure and properties of lattice defects, in particular those which are intimately related to the nature of bonding. Moreover, the potentials of the same type can be developed using the same approach for other bcc transition metals, as well as for alloys and compounds based on them.

ACKNOWLEDGMENTS

This research was supported by the U.S. Department of Energy, BES Grant no. DE-PG02-98ER45702 (M.M., V.V.). The computations were supported in part by the Materials Modelling Laboratory, Department of Materials, Oxford University, on the Hewlett Packard computers that were jointly funded by Hewlett Packard and Higher Education Funding Council of UK under the Joint Equipment Research Initiative scheme. D.N.-M. and D.G.P. would also like to acknowledge the Oxford University Supercomputing Centre for the use of its facilities.

*Present address: IZBS, University of Karlsruhe, Karlsruhe, D-76131, Germany.
Electronic address: matous@alumni.upenn.edu
†Present address: Theory and Modelling Department, Culham Science Centre, UKAEA, Oxfordshire, OX14 3DB, United Kingdom.
Electronic address: duc.nguyen@ukaea.org.uk
‡Electronic address: vitek@lrsm.upenn.edu

[1] V. Vitek, in *Dislocations and Properties of Real Materials*, edited by M. Lorretto (The Institute of Metals, London, 1985), p. 30.
[2] M.S. Duesbery and G.Y. Richardson, CRC Crit. Rev. Solid State Mater. Sci. **17**, 1 (1991).
[3] V. Vitek, Prog. Mater. Sci. **36**, 1 (1992).
[4] J.W. Christian, in *Proc. 3rd Int. Conf. on Reinstoffe in Wissenschaft und Technik* (Akademie-Verlag, Berlin, 1970), p. 263.
[5] L.P. Kubin, Rev. Deform. Behav. Mater. **4**, 181 (1982).
[6] J.W. Christian, Metall. Trans. A **14A**, 1237 (1983).
[7] M.S. Duesbery, *Dislocations in Solids* (North-Holland, Amsterdam, 1989), Vol. 8, p. 67.
[8] G. Taylor, Prog. Mater. Sci. **36**, 29 (1992).
[9] A.F. Voter, MRS Bull. **21**, 17 (1996).
[10] M.S. Daw and M.I. Baskes, Phys. Rev. B **29**, 6443 (1984).
[11] M.S. Daw, S.M. Foiles, and M.I. Baskes, Mater. Sci. Rep. **9**, 251 (1993).
[12] M.W. Finnis and J.E. Sinclair, Philos. Mag. A **50**, 45 (1984).
[13] G.J. Ackland, G. Tichy, V. Vitek, and M.W. Finnis, Philos. Mag. A **56**, 735 (1987).
[14] R.W. Cahn, A.G. Evan, and M. Mclean, *High-Temperature Structural Materials* (Chapman & Hall, London, 1996).
[15] J.J. Petrovic and A.K. Vasudevan, Mater. Sci. Eng., A **261**, 1 (1999).
[16] N.S. Stoloff, C.T. Liu, and S.C. Deevi, Intermetallics **8**, 1313 (2000).
[17] F. Caruso, Adv. Mater. **13**, 11 (2001).
[18] J.H. Westbrook and R.L. Fleisher, *Intermetallic Compounds: Principles and Practice* (Wiley, New York, 2002).
[19] J. Friedel, in *The Physics of Metals*, edited by J.M. Ziman (Cambridge University Press, Cambridge, 1969), p. 340.
[20] D.G. Pettifor, *Bonding and Structure of Molecules and Solids* (Oxford University Press, New York, 1995).
[21] C. Woodward, J.M. MacLaren, and S.I. Rao, J. Mater. Res. **7**, 1735 (1992).
[22] Y. Song, S.P. Tang, J.H. Xu, O.N. Mryasov, A.J. Freeman, C. Woodward, and D.M. Dimiduk, Philos. Mag. B **70**, 987 (1994).
[23] A.K. McMahan and J.E. Klepeis, *Tight-Binding Approach to Computational Materials Science* (Materials Research Society, Pittsburg, 1998).
[24] M.H. Yoo and C.L. Fu, Metall. Mater. Trans. A **29A**, 49 (1998).
[25] G.J. Ackland and R. Thetford, Philos. Mag. A **56**, 15 (1987).
[26] M.S. Duesbery and V. Vitek, Acta Mater. **46**, 1481 (1998).
[27] K. Ito and V. Vitek, Philos. Mag. A **81**, 1387 (2001).
[28] V. Vitek, Cryst. Lattice Defects **5**, 1 (1975).
[29] C. Woodward and S.I. Rao, Philos. Mag. A **81**, 1305 (2001).
[30] M.I. Baskes, Phys. Rev. B **46**, 2727 (1992).
[31] J.A. Moriarty, Phys. Rev. B **42**, 1609 (1990).
[32] J.A. Moriarty, Phys. Rev. B **49**, 12 431 (1994).
[33] D.G. Pettifor, Phys. Rev. Lett. **63**, 2480 (1989).
[34] D.G. Pettifor, in *Many Atom Interactions in Solids*, edited by R.M. Nieminen, J. Puska, and M. Manninen, Springer Reports in Physics, Vol. 48 (Springer, Berlin, 1990), p. 64.
[35] D.G. Pettifor and I.I. Oleinik, Comput. Mater. Sci. **23**, 33 (2002).
[36] A.P. Horsfield, A.M. Bratkovsky, D.G. Pettifor, and M. Aoki, Phys. Rev. B **53**, 1656 (1996).
[37] A. Girshick, A.M. Bratkovsky, D.G. Pettifor, and V. Vitek, Philos. Mag. A **77**, 981 (1998).

[38] A. Girshick, D.G. Pettifor, and V. Vitek, Philos. Mag. A **77**, 999 (1998).
[39] S. Znam, D. Nguyen-Manh, D.G. Pettifor, and V. Vitek, Philos. Mag. **83**, 415 (2003).
[40] J.C. Slater and G.F. Koster, Phys. Rev. **94**, 1498 (1954).
[41] R.E. Cohen, M.J. Mehl, and D.A. Papaconstantopoulos, Phys. Rev. B **50**, 14 694 (1994).
[42] M.H.F. Sluiter and P.P. Singh, Phys. Rev. B **49**, 10 918 (1994).
[43] M.J. Mehl and D.A. Papaconstantopoulos, Phys. Rev. B **54**, 4519 (1996).
[44] M.S. Tang, C.Z. Wang, C.T. Chan, and K.M. Ho, Phys. Rev. B **53**, 979 (1996).
[45] H. Haas, C.Z. Wang, M. Fahnle, C. Elsässer, and K.M. Ho, Phys. Rev. B **57**, 1461 (1998).
[46] C.Z. Wang, B.C. Pan, and K.M. Ho, J. Phys.: Condens. Matter **11**, 2043 (1999).
[47] D. Nguyen-Manh, D.G. Pettifor, and V. Vitek, Phys. Rev. Lett. **85**, 4136 (2000).
[48] D.G. Pettifor and I.I. Oleinik, Phys. Rev. B **59**, 8487 (1999).
[49] D.G. Pettifor and I.I. Oleinik, Phys. Rev. Lett. **84**, 4124 (2000).
[50] O.K. Andersen, A. Arcangeli, R.W. Tank, T. Saha-Dasgusta, G. Krier, O. Jepsen, and I. Dasgusta, in *Tight-Binding Approach to Computational Materials Science*, edited by P.E.A. Turchi, A. Gonis, and L. Colombo, Mater. Res. Soc. Symp. Proc. **491** (Materials Research Society, Pittsburg, 1998), p. 3.
[51] C. Woodward and S.I. Rao, Phys. Rev. Lett. **88**, 216402 (2002).
[52] M. Mrovec, V. Vitek, D. Nguyen-Manh, D.G. Pettifor, L.G. Wang, and M. Šob, in *Multiscale Modelling of Materials*, edited by T. Diaz de la Rubia, T. Kaxiras, V. Bulatov, N. M. Ghoniem, and R. Phillips, Mater. Res. Soc. Symp. Proc. **538** (Materials Research Society, Pittsburgh, 1999), p. 529.
[53] M. Mrovec, V. Vitek, D. Nguyen-Manh, D.G. Pettifor, L.G. Wang, and M. Šob, in *Multiscale Phenomena in Materials–Experiments and Modeling*, edited by D.H. Lassila, I.M. Robertson, R. Phillips, and B. Devincre, Mater. Res. Soc. Symp. Proc. **578** (Materials Research Society, Pittsburgh, 2000), p. 199.
[54] M. Mrovec, Ph.D. thesis, University of Pennsylvania, 2002.
[55] M. Aoki, P. Gumbsch, and D.G. Pettifor, in *Interatomic Potentials and Structural Stability*, edited by T. Terakura and H. Akai (Springer, Berlin, 1993), Vol. 114, p. 23.
[56] D.G. Pettifor, J. Phys. F: Met. Phys. **8**, 219 (1978).
[57] D. Nguyen-Manh, D.G. Pettifor, S. Znam, and V. Vitek, in *Tight-Binding Approach to Computational Materials Science*, Ref. 50, pp. 353–358.
[58] A.P. Sutton, M.W. Finnis, D.G. Pettifor, and Y. Ohta, J. Phys. C **21**, 35 (1988).
[59] H. Nakamura, D. Nguyen-Manh, and D.J. Pettifor, J. Alloys Compd. **306**, 113 (2000).
[60] L. Goodwin, A.J. Skinner, and D.G. Pettifor, Europhys. Lett. **9**, 701 (1989).
[61] O.K. Andersen, O. Jepsen, and M. Šob, in *Electronic Band Structure and Its Applications*, edited by M. Yussouff (Springer, New York, 1987), p. 1.
[62] M. Šob and V. Vitek, in *Stability of Materials: NATO Advanced Science Institute Series*, edited by A. Gonis, P.E.A. Turschi, and J. Kudrnovsky (Plenum Press, New York, 1996), p. 449.
[63] C. Kittel, *Introduction to Solid State Physics* (Wiley, New York, 1986).
[64] P. Bujard, Ph.D. thesis, University of Geneva, 1982.
[65] V. Paidar, L.G. Wang, M. Šob, and V. Vitek, Modell. Simul. Mater. Sci. Eng. **7**, 369 (1999).
[66] M. Šob (private communication).
[67] P. Blaha, K. Schwartz, P. Sorantin, and S.B. Trickey, Comput. Phys. Commun. **59**, 399 (1990).
[68] E.C. Bain, Trans. AIME **70**, 25 (1924).
[69] S.M. Foiles, Phys. Rev. B **48**, 4287 (1993).
[70] W. Xu and J.A. Moriarty, Phys. Rev. B **54**, 6941 (1996).
[71] B. Meyer and M. Fähnle, Phys. Rev. B **56**, 13 595 (1997).
[72] P. Söderlind, L.H. Yang, J.A. Moriarty, and J.M. Wills, Phys. Rev. B **61**, 2579 (2000).
[73] K. Kunc, *Electronic Structure Dynamics and Quantum Structure Properties of Condensed Matter* (Plenum, New York, 1985).
[74] B.M. Powel, P. Martel, and A.D.B. Woods, Can. J. Phys. **55**, 1601 (1977).
[75] M.W. Finnis, K.L. Kear, and D.G. Pettifor, Phys. Rev. Lett. **52**, 291 (1984).
[76] A.D.B. Woods, B.N. Brockhouse, R.H. March, and A.T. Stewarrt, Phys. Rev. **128**, 1112 (1962).
[77] P.B. Hirsch, in *Proceedings of the Fifth International Conference on Crystallography* (Cambridge University Press, Cambridge, 1960), p. 139.
[78] H. Suzuki, in *Dislocation Dynamics*, edited by A. Rosenfield, G. Hahn, A. Bement, and R. Jaffee (McGraw-Hill, New York, 1968), p. 679.
[79] W. Siegle, Philos. Mag. A **79**, 1009 (1999).
[80] M.S. Duesbery, V. Vitek, and J. Cserti, in *Understanding Materials: Professor Sir Peter Hirsch Festschrift*, edited by C.J. Humphreys (The Institute of Materials, London, 2002), p. 165.
[81] W. Xu and J.A. Moriarty, Comput. Mater. Sci. **9**, 348 (1998).
[82] K. Masuda and A. Sato, Philos. Mag. B **37**, 531 (1978).
[83] K. Masuda, K. Kobayashi, A. Sato, and T. Mori, Philos. Mag. B **43**, 19 (1981).
[84] S. Ismail-Beigi and T.A. Arias, Phys. Rev. Lett. **84**, 1499 (2000).
[85] V. Vitek, Philos. Mag. A **18**, 773 (1968).
[86] C. Woodward (private communication).
[87] J.P. Hirth and J. Lothe, *Theory of Dislocations* (Wiley-Interscience, New York, 1982).
[88] J.L. Bassani, K. Ito, and V. Vitek, Mater. Sci. Eng., A **319**, 97 (2001).